Inorg. Chem. **2005**, *44*, 9314–9321

Luminescent Lanthanide Selenites and Tellurites Decorated by MoO_4 Tetrahedra or MoO_6 Octahedra: $Nd_2MoSe_2O_{10}$, $Gd_2MoSe_3O_{12}$, $La_2MoTe_3O_{12}$, and $Nd_2MoTe_3O_{12}$

Yue-Ling Shen,[†] Hai-Long Jiang,[†] Jian Xu,[‡] Jiang-Gao Mao,*[,†] and Kok Wai Cheah[‡]

State Key Laboratory of Structure Chemistry, Fujian Institute of Research on the Structure of Matter, The Chinese Academy of Sciences, and The Graduate School of Chinese Academy of Sciences, Fuzhou 350002, P. R. China, and Department of Physics, Centre for Advanced Luminescence Materials, Hong Kong Baptist University, Kowloon Tong, Hong Kong, P. R. China

Received August 11, 2005

Solid state reactions of lanthanide oxide, MoO_3 and SeO_2 (or TeO_2) at high temperature in an evacuated quartz tube lead to four new Ln–Mo–Se(Te)–O quaternary phases with four different types of structures, namely, $Nd_2MoSe_2O_{10}$, $Gd_2MoSe_3O_{12}$, $La_2MoTe_3O_{12}$, and $Nd_2MoTe_3O_{12}$. The structure of $Nd_2MoSe_2O_{10}$ features a 3D architecture built by the intergrowth of the Nd–Se–O layers with the Nd–Mo–O layers. The structure of $Gd_2MoSe_3O_{12}$ contains a 3D network of gadolinium selenite with the MoO_6 octahedra occupying the cavities of the structure. The structure of $La_2MoTe_3O_{12}$ features a 3D network of $La_2(Te_3O_8)^{2+}$ with the tunnels along the *a* axis occupied by the MoO_4 tetrahedra. $Nd_2MoTe_3O_{12}$ features a 2D layer built by the lanthanide ions interconnected by tellurite groups and ditellurite groups, with the MoO_4 tetrahedra as the interlayer pendant groups. Room temperature and low temperature luminescent studies indicate that $Nd_2MoSe_2O_{10}$ and $Nd_2MoTe_3O_{12}$ exhibit strong luminescence in the near-IR region.

Introduction

Selenites and tellurites can adopt many unusual structures due to the presence of the stereochemically active lone pair electrons.[1] The asymmetric coordination polyhedron adopted by the Se(IV) or Te(IV) atom may result in noncentrosymmetric structures with consequent interesting physical properties, such as nonlinear optical second harmonic generation (SHG).[2−4] Transition metal ions with d^0 electronic configuration (such as Ti^{4+}, Nb^{5+}, W^{6+}, Mo^{6+}, etc.) are susceptible to second-order Jahn−Teller distortions, and they have been introduced to the selenite or tellurite systems in order to obtain compounds with good SHG properties.[2−4] Most of these research efforts have been focused on alkali and alkaline earth compounds.[2−4] Although a number of lanthanide selenites and tellurium(IV) oxides have been reported,[1,5,6] reports on lanthanide selenites or tellurium(IV) oxides with additional transition metal ions are still rare.[1,7] Lanthanide compounds such as Er(III) and Nd(III) compounds exhibit good luminescent properties in the near-IR region which are important in applications as optical signal amplifiers and lasers.[8] It is hoped that the use of two types of anions (SeO_3^{2-} or TeO_3^{2-} anion and Mo(VI) oxygen

* To whom correspondence should be addressed. E-mail: mjg@ms.fjirsm.ac.cn.

[†] The Chinese Academy of Sciences and The Graduate School of the Chinese Academy of Sciences.

[‡] Hong Kong Baptist University.

(1) (a) Wickleder, M. S. *Chem. Rev.* **2002**, *102*, 2011 and references therein.
(2) (a) Ra, H.-S.; Ok, K.-M.; Halasyamani, P. S. *J. Am. Chem. Soc.* **2003**, *125*, 7764. (b) Ok, K.-M.; Halasyamani, P. S. *Inorg. Chem.* **2004**, *43*, 4248.
(3) (a) Hart, R. T.; Ok, K.-M.; Halasyamani, P. S.; Zwanziger, J. W. *Appl. Phys. Lett.* **2004**, *85*, 938. (b) Goodey, J.; Broussard, J.; Halasyamani, P. S. *Chem. Mater.* **2002**, *14*, 3174.
(4) (a) Johnston, M. G.; Harrison, W. T. A. *Inorg. Chem.* **2001**, *40*, 6518. (b) Balraj, V.; Vidyasagar, K. *Inorg. Chem.* **1999**, *38*, 5809.
(5) (a) Wontcheu, J.; Schleid, T. *J. Solid State Chem.* **2003**, *171*, 429. (b) Wontcheu, J.; Schleid, T. *Z. Anorg. Allg. Chem.* **2002**, *628*, 1941. (c) Ruck, M.; Schmidt, P. *Z. Anorg. Allg. Chem.* **2003**, *629*, 2133. (d) Wontcheu, J.; Schleid, T. *Z. Anorg. Allg. Chem.* **2003**, *629*, 1463.
(6) (a) Meier, S. F.; Schleid, T. *Z. Anorg. Allg. Chem.* **2002**, *628*, 1941. (b) Shen, Y. L.; Mao, J. G. *J. Alloy Compd.* **2004**, *385*, 86.
(7) (a) Shen, Y.-L.; Mao, J.-G. *Inorg. Chem.* **2005**, *44*, 5328. (b) Wickleder, M. S.; Hamida, M. B. *Z. Anorg. Allg. Chem.* **2003**, *629*, 556. (c) Harrison, W. T. A.; Zhang, Z. H. *J. Solid State Chem.* **1997**, *133*, 572.
(8) (a) Slooff, L. H.; Polman, A.; Oude Wolbers, M. P.; van Veggel, F. C. J. M.; Reinhoudt, D. N.; Hofstraat, J. W. *J. Appl. Phys.* **1997**, *83*, 497.

10.1021/ic051376m CCC: $30.25
Published on Web 11/02/2005

Table 1. Crystal Data and Structure Refinements for the Four Compounds

	$Nd_2MoSe_2O_{10}$	$Gd_2MoSe_3O_{12}$	$La_2MoTe_3O_{12}$	$Nd_2MoTe_3O_{12}$
fw	702.34	839.32	948.56	959.22
space group	$P\bar{1}$	$P\bar{1}$	*Pnma*	*Pnma*
a, Å	5.3582(7)	6.557(1)	7.3150(6)	17.701(2)
b, Å	6.892(1)	7.117(2)	11.7110(9)	11.359(1)
c, Å	12.576(3)	10.879(2)	13.602(1)	5.3230(4)
α, deg	85.80(1)	85.225(6)	90	90
β, deg	83.97(1)	72.752(5)	90	90
γ, deg	70.07(1)	86.546(6)	90	90
V, Å^3	433.9(2)	482.8(2)	1165.1(2)	1070.3(2)
Z	2	2	4	4
D_{calcd}, g·cm^{-3}	5.376	5.773	5.407	5.953
μ, mm^{-1}	21.641	26.229	15.679	18.787
GOF on F^2	1.039	1.022	1.395	1.184
R1, wR2 ($I > 2\sigma(I)$)[a]	0.0405, 0.1021	0.0301, 0.0698	0.0479, 0.0622	0.0325, 0.0648
R1, wR2 (all data)	0.0440, 0.1038	0.0347, 0.0720	0.0528, 0.0633	0.0380, 0.0667

[a] $R1 = \sum||F_o| - |F_c||/\sum|F_o|$, $wR2 = \{\sum w[(F_o)^2 - (F_c)^2]^2/\sum w[(F_o)^2]^2\}^{1/2}$.

anion) for activation the lanthanide(III) ions can improve their luminescent properties. Our research efforts with this aspect lead to four new lanthanide selenites and tellurites (or polytellurites) containing MoO_4 tetrahedra or MoO_6 octahedra, namely, $Nd_2MoSe_2O_{10}$, $Gd_2MoSe_3O_{12}$, $La_2MoTe_3O_{12}$, and $Nd_2MoTe_3O_{12}$. Herein we report their syntheses, crystal structures, and luminescent properties.

Experimental Section

Materials and Instrumentation. All chemicals were obtained from commercial sources and were used without further purification. X-ray powder diffraction (XRD) patterns (Cu Kα) were collected in a sealed glass capillary on a XPERT-MPD $\theta-2\theta$ diffractometer. IR spectra were recorded on a Magna 750 FT-IR spectrometer photometer as KBr pellets in the 4000−400 cm^{-1} region. The luminescence lifetimes for $Nd_2MoSe_2O_{10}$ and $Nd_2MoTe_3O_{12}$ were measured at room temperature with a pulsed Q-switched Nd:YAG laser (λ=355 nm, Quantel Brilliant B) as a light source. The luminescent signal was dispersed through a 0.5 m focal length Acton monochromator with 1200 line/mm grating. The data were collected by a cooled PMT (Hamamatsu, R636-10) detector and then captured by an Agilent Infiniium oscilloscope (600 MHZ, 4 GSa/s). The IR emission measurements employed the 514.2 nm line of an Ar ion laser (Spectral Physics Stabilite 2017) as excitation light, using the same 0.5 m focal length Acton monochromator, but with 1200 line/mm or 300 line/mm gratings. The signal was detected by a liquid nitrogen cooled InSb IR detector (EG&G). For low-temperature measurements, the samples were mounted in a closed-cycle cryostat (Oxford Instruments CC1104). All spectra were taken through a 780 nm cutoff filter. For all luminescent measurements, three independent experiments have been performed, and the results are reproducible. Magnetic susceptibility measurements on polycrystalline samples were performed with a PPMS-9T magnetometer at a field of 10000 Oe in the range 2−300 K.

Preparation of $Nd_2MoSe_2O_{10}$. $Nd_2MoSe_2O_{10}$ was obtained in our attempt to prepare a Nd−Cu−Mo−Se−O phase. Light purple single crystals of $Nd_2MoSe_2O_{10}$ were initially obtained by reaction of a mixture of Nd_2O_3 (0.1347 g, 0.4 mmol), MoO_3 (0.0578 g, 0.4 mmol), $CuCl_2$ (0.0536 g, 0.4 mmol), and SeO_2 (0.1780 g, 1.6 mmol) which was ground, pressed into a pellet, and sealed in an evacuated quartz tube at 750 °C for 7 days. Results of single-crystal X-ray diffraction studies indicate the absence of Cu and Cl elements in $Nd_2MoSe_2O_{10}$; hence, the compound was then resynthesized without the addition of $CuCl_2$. The pure phase of $Nd_2MoSe_2O_{10}$ was obtained by reaction of a mixture of Nd_2O_3 (0.2019 g, 0.6 mmol), MoO_3 (0.0862 g, 0.6 mmol), and SeO_2 (0.1329 g, 1.2 mmol) at 700 °C for 6 days.

Preparation of $Gd_2MoSe_3O_{12}$. Light yellow single crystals of $Gd_2MoSe_3O_{12}$ were prepared in a procedure similar to that of $Nd_2MoSe_2O_{10}$, using Gd_2O_3 (0.1452 g, 0.4 mmol) instead of Nd_2O_3. Efforts to synthesize a pure powder sample of $Gd_2MoSe_3O_{12}$ were unsuccessful; hence, single crystals that were manually selected were used for its XRD and IR studies.

Preparation of $La_2MoTe_3O_{12}$. Colorless crystals of $La_2MoTe_3O_{12}$ were obtained by solid-state reaction of La_2O_3 (0.0978 g, 0.3 mmol), MoO_3 (0.0864 g, 0.6 mmol), and TeO_2 (0.2400 g, 1.5 mmol) in an evacuated quartz tube at 750 °C for 7 days. After proper structural determinations, a pure powder sample was synthesized from a mixture of La_2O_3 (0.1306 g, 0.4 mmol), MoO_3 (0.0580 g, 0.4 mmol), and TeO_2 (0.1918 g, 1.2 mmol) at 700 °C for 7 days.

Preparation of $Nd_2MoTe_3O_{12}$. Light purple $Nd_2MoTe_3O_{12}$ was obtained by the solid state reaction of a mixture of Nd_2O_3 (0.0673 g, 0.2 mmol), MoO_3 (0.0863 g, 0.6 mmol), and TeO_2 (0.1914 g, 1.2 mmol) in an evacuated quartz tube at 700 °C for 6 days. The pure powder sample was synthesized from a mixture of Nd_2O_3 (0.1006 g, 0.3 mmol), MoO_3 (0.0432 g, 0.3 mmol), and TeO_2 (0.1437 g, 0.9 mmol) at 700 °C for 7 days. For powder samples of $Nd_2MoSe_2O_{10}$, $La_2MoTe_3O_{12}$, and $Nd_2MoTe_3O_{12}$, their measured X-ray powder patterns match with XRD powder patterns simulated from their single-crystal data. Thus, these powder samples are single phases and were used for subsequent luminescent and IR studies.

Single-Crystal Structure Determination. Single crystals of $Nd_2MoSe_2O_{10}$, $Gd_2MoSe_3O_{12}$, $La_2MoTe_3O_{12}$, and $Nd_2MoTe_3O_{12}$ were mounted on a Rigaku Mercury CCD diffractometer equipped with graphite-monochromated Mo Kα radiation (λ = 0.71073 Å). Intensity data were collected by the narrow frame method at 293 K. The data sets were corrected for Lorentz and polarization factors as well as for absorption by the multiscan method.[9] All four structures were solved by the direct methods and refined by full-matrix least-squares fitting on F^2 by SHELX-97.[9] All atoms except O(4) of $Nd_2MoTe_3O_{12}$ were refined anisotropically. Crystallographic data and structural refinements for the four compounds are summarized in Table 1. Important bond distances and angles are listed in Table 2. More details on the crystallographic studies as well as atom displacement parameters are given as Supporting Information.

(9) (a) *CrystalClear* ver. 1.3.5; Rigaku Corp.: Woodlands, TX, 1999. (b) Sheldrick, G. M. *SHELXTL, Crystallographic Software Package, SHELXTL*, version 5.1; Bruker-AXS: Madison, WI, 1998.

Table 2. Important Bond Lengths [Å] for the Four Compounds[a]

	$Nd_2MoSe_2O_{10}$		
Nd(1)−O(9)#1	2.407(7)	Nd(1)−O(5)#2	2.426(7)
Nd(1)−O(7)#3	2.458(7)	Nd(1)−O(9)	2.458(6)
Nd(1)−O(10)	2.495(8)	Nd(1)−O(7)#4	2.512(7)
Nd(1)−O(8)#5	2.514(7)	Nd(1)−O(5)	2.529(7)
Nd(2)−O(4)#6	2.407(7)	Nd(2)−O(2)#7	2.409(7)
Nd(2)−O(10)	2.420(7)	Nd(2)−O(4)#8	2.443(8)
Nd(2)−O(6)	2.462(7)	Nd(2)−O(1)#9	2.484(7)
Nd(2)−O(8)#5	2.489(8)	Nd(2)−O(3)	2.540(7)
Mo(1)−O(2)	1.740(7)	Mo(1)−O(1)	1.752(7)
Mo(1)−O(3)	1.764(7)	Mo(1)−O(4)	1.816(6)
Se(1)−O(9)	1.704(7)	Se(1)−O(8)	1.713(6)
Se(1)−O(10)	1.730(6)	Se(2)−O(6)	1.680(7)
Se(2)−O(7)	1.723(6)	Se(2)−O(5)	1.754(6)
	$Gd_2MoSe_3O_{12}$		
Gd(1)−O(1)#1	2.351(13)	Gd(1)−O(9)#2	2.360(13)
Gd(1)−O(10)#3	2.392(13)	Gd(1)−O(4)#4	2.400(12)
Gd(1)−O(4)#5	2.436(12)	Gd(1)−O(9)	2.459(13)
Gd(1)−O(6)	2.461(11)	Gd(1)−O(5)#3	2.493(12)
Gd(2)−O(11)#6	2.350(13)	Gd(2)−O(8)	2.348(12)
Gd(2)−O(12)#1	2.394(13)	Gd(2)−O(5)#3	2.384(12)
Gd(2)−O(7)#7	2.419(12)	Gd(2)−O(2)#1	2.421(14)
Gd(2)−O(3)	2.481(12)	Gd(2)−O(1)#1	2.488(12)
Mo(1)−O(11)	1.725(13)	Mo(1)−O(10)	1.773(13)
Mo(1)−O(12)	1.777(13)	Mo(1)−O(3)	2.120(12)
Mo(1)−O(7)#7	2.186(12)	Mo(1)−O(6)#3	2.361(11)
Se(1)−O(2)	1.677(5)	Se(1)−O(1)	1.720(5)
Se(1)−O(3)	1.756(5)	Se(2)−O(4)	1.705(5)
Se(2)−O(6)	1.713(5)	Se(2)−O(5)	1.728(5)
Se(3)−O(8)	1.666(5)	Se(3)−O(7)	1.742(5)
Se(3)−O(9)	1.745(5)		
	$La_2MoTe_3O_{12}$		
La(1)−O(1)#1	2.451(8)	La(1)−O(4)#2	2.477(7)
La(1)−O(2)	2.500(8)	La(1)−O(6)#3	2.524(8)
La(1)−O(5)	2.545(7)	La(1)−O(1)#4	2.610(8)
La(1)−O(8)	2.634(8)	La(1)−O(2)#4	2.681(9)
La(1)−O(3)#2	2.821(8)	Te(1)−O(1)	1.848(8)
Te(1)−O(2)	1.858(8)	Te(1)−O(3)	1.898(8)
Te(2)−O(4)	1.869(12)	Te(2)−O(5)	1.882(11)
Te(2)−O(3)	2.183(7)	Te(2)−O(3)#5	2.183(7)
Mo(1)−O(6)#5	1.754(8)	Mo(1)−O(6)	1.754(8)
Mo(1)−O(7)	1.755(14)	Mo(1)−O(8)	1.793(11)
	$Nd_2MoTe_3O_{12}$		
Nd(1)−O(4)#1	2.324(4)	Nd(1)−O(8)#2	2.334(4)
Nd(1)−O(7)	2.396(3)	Nd(1)−O(5)#3	2.460(4)
Nd(1)−O(8)#3	2.524(4)	Nd(1)−O(2)#2	2.547(3)
Nd(1)−O(3)	2.567(4)	Nd(1)−O(5)	2.603(4)
Mo(1)−O(1)	1.716(6)	Mo(1)−O(3)#4	1.782(4)
Mo(1)−O(3)	1.782(4)	Mo(1)−O(2)	1.802(5)
Te(1)−O(4)	1.838(4)	Te(1)−O(5)	1.891(4)
Te(1)−O(6)	1.987(2)	Te(2)−O(8)#4	1.882(3)
Te(2)−O(8)	1.882(3)	Te(2)−O(7)	1.902(5)

[a] Symmetry transformations used to generate equivalent atoms: for $Nd_2MoSe_2O_{10}$, #1 $-x, -y+1, -z$, #2 $-x, -y+2, -z$, #3 $x, y-1, z$, #4 $-x+1, -y+2, -z$, #5 $x+1, y, z$, #6 $-x+1, -y+2, -z+1$, #7 $-x+1, -y+1, -z+1$, #8 $x-1, y, z$, #9 $-x, -y+2, -z+1$; for $Gd_2MoSe_3O_{12}$, #1 $x+1, y, z$, #2 $-x+1, -y+2, -z+2$, #3 $-x+1, -y+1, -z+2$, #4 $-x+2, -y+1, -z+2$, #5 $x, y+1, z$, #6 $-x+1, -y+1, -z+1$, #7 $x, y-1, z$; for $La_2MoTe_3O_{12}$, #1 $-x+1/2, -y+1, z+1/2$, #2 $x+1/2, y, -z+1/2$, #3 $-x, -y+1, -z+1$, #4 $x-1/2, y, -z+1/2$ #5 $x, -y+3/2, z$; for $Nd_2MoTe_3O_{12}$, #1 $-x+1, -y, -z+2$, #2 $x, y, z+1$, #3 $-x+1, -y, -z+1$, #4 $x, -y+1/2, z$.

Results and Discussion

Structural Descriptions. $Nd_2MoSe_2O_{10}$, $Gd_2MoSe_3O_{12}$, $La_2MoTe_3O_{12}$, and $Nd_2MoTe_3O_{12}$ represent the first examples of lanthanide selenium(IV) or tellurium(IV) oxides decorated by MoO_4 tetrahedra or MoO_6 octahedra. They belong to four different structural types.

$Nd_2MoSe_2O_{10}$ can also be formulated as $Nd_2(MoO_4)(SeO_3)_2$. The structure of $Nd_2MoSe_2O_{10}$ features a 3D network in which the Nd(III) ions are interconnected by SeO_3^{2-} anions and MoO_4 tetrahedra. Both Nd(1) and Nd(2) are 8-coordinated by eight oxygen atoms (Figure 1). The Nd−O distances are in the range 2.407(7)−2.540(7) Å (Table 2), comparable to those reported in other neodymium(III) selenites.[10] The Mo atom is in a slightly distorted tetrahedral coordination environment with Mo−O distances in the range 1.740(7)−1.816(6) Å (Table 2). The coordination geometry around both Se(1) and Se(2) can be described as a SeO_3 trigonal pyramid. The Se−O distances are in the range 1.680(7)−1.754(6) Å. Bond valence calculations indicate that the Mo atom is in an oxidation state of +6 and the Se atoms are +4; the calculated total bond valences for Mo(1), Se(1), and Se(2) are 5.84, 3.88, and 3.86, respectively.[11]

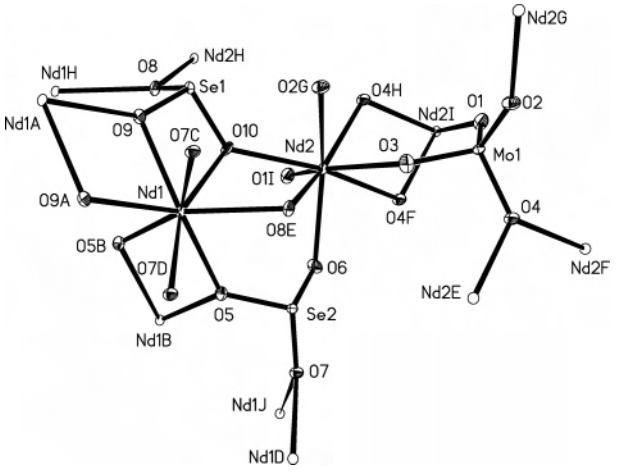

Figure 1. ORTEP representation of the selected unit in $Nd_2MoSe_2O_{10}$. The thermal ellipsoids are drawn at 50% probability. Symmetry codes for generated atoms: (a) $-x, -y+1, -z$; (b) $-x, -y+2, -z$; (c) $x, y-1, z$; (d) $-x+1, -y+2, -z$; (e) $x+1, y, z$; (f) $-x+1, -y+2, -z+1$; (g) $-x+1, -y+1, -z+1$; (h) $x-1, y, z$; (i) $-x, -y+2, -z+1$; (j) $x, y+1, z$.

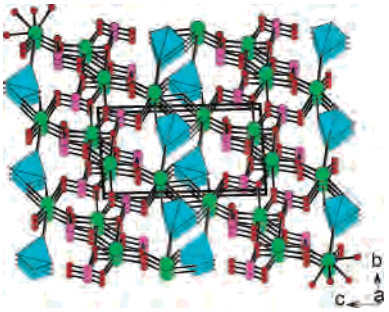

Figure 2. View of the structure of $Nd_2MoSe_2O_{10}$ down the *a* axis. The MoO_4 tetrahedra are shaded in cyan. Nd, Se, and O atoms are drawn as green, pink, and red circles, respectively.

The interconnection of Nd(1) atoms via bridging selenite groups leads to a ⟨001⟩ layer (Figure 2), whereas Nd(2) atoms are bridged by MoO_4 tetrahedra to form a ⟨002⟩ layer (Figure 2). The above two types of layers are further interconnected via the Nd−O (selenite) bonds (Nd(2)−O(6), Nd(2)−O(8),

(10) (a) Stancheva, M.; Petrova, R.; Macicek, J. *Acta Crystallogr.* **1998**, *C54*, 699. (b) Depedro, M.; Enjalbert, R.; Castro, A.; Trombe, J. C.; Galy, J. *J. Solid State Chem.* **1994**, *108*, 87. (c) Wickleder, M. S. *Z. Naturforsch.* **2002**, *B57*, 1414.

(11) (a) Brese, N. E.; O'Keeffe, M. *Acta Crystallogr.* **1991**, *B47*, 192. (b) Brown, I. D.; Altermatt, D. *Acta Crystallogr.* **1985**, *B41*, 244.

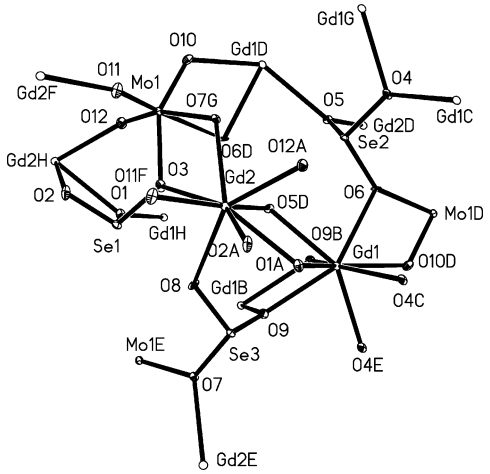

Figure 3. ORTEP representation of the selected unit in $Gd_2MoSe_3O_{12}$. The thermal ellipsoids are drawn at 50% probability. Symmetry codes for the generated atoms: (a) $x + 1, y, z$; (b) $-x + 1, -y + 2, -z + 2$; (c) $-x + 2, -y + 1, -z + 2$; (d) $-x + 1, -y + 1, -z + 2$; (e) $x, y + 1, z$; (f) $-x + 1, -y + 1, -z + 1$; (g) $x, y - 1, z$; (h) $x - 1, y, z$.

and Nd(2)−O(10)) into a 3D network (Figure 2). The selenite group containing Se(1) chelates with a Nd(1) atom and also bridges with two Nd(1) and two Nd(2) atoms. The selenite group composed of the Se(2) atom bridges with four Nd(1) and one Nd(2) atoms. The MoO_4 tetrahedron connects with five Nd(2) atoms. The lone pairs of the selenium(IV) atoms are oriented to the cavities of the structure. The effective volume of the lone pair is approximately the same as the volume of an O^{2-} anion according to Galy and Andersson.[12]

With the molar ratio of Se/Ln increased to 3:2, $Gd_2MoSe_3O_{12}$ with a different structure was obtained. $Gd_2MoSe_3O_{12}$ can also be formulated as $Gd_2(MoO_3)(SeO_3)_3$, which can be considered as one O^{2-} anion of $Nd_2MoSe_2O_{10}$ being replaced by the third selenite group. The structure of $Gd_2MoSe_3O_{12}$ features a 3D network of gadolinium selenite with the MoO_6 octahedra occupying the cavities of the network. Both gadolinium atoms in the asymmetric unit are 8-coordinated with Gd−O distances ranging from 2.337(5) to 2.485(5) Å, comparable to those reported in other gadolinium selenites.[7a,13] Unlike that in $Nd_2MoSe_2O_{10}$, the molybdenum atom in $Gd_2MoSe_3O_{12}$ is octahedrally coordinated by three oxygen atoms from three selenite groups and three O^{2-} anions (Figure 3). The MoO_6 octahedron is severely distorted, and the three Mo−O (selenite) distances (2.111(6)−2.353(5) Å) are significantly longer than those of three Mo−O (O^{2-}) (1.736(6)−1.752(5) Å) (Table 2). The O−Mo−O angles are also greatly deviated from 180° and 90°. The Mo atom is distorted toward an face formed by O(10), O(11), and O(12) atoms (local C_3 direction) but is distorted away from the oxide ligands that bridge to the lone pair cations, Se(IV).[14] Taking into account the six Mo−O bond lengths as well as the deviations from 180° of the three trans O−Mo−O bond angles, the magnitude of the distortion (Δ_d) was calculated to be 1.492, which is comparable to those

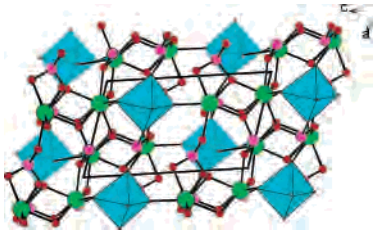

Figure 4. View of the structure of $Gd_2MoSe_3O_{12}$ down the *b* axis. The MoO_6 octahedra are shaded in cyan. Gd, Se, and O atoms are drawn as green, pink, and red circles, respectively.

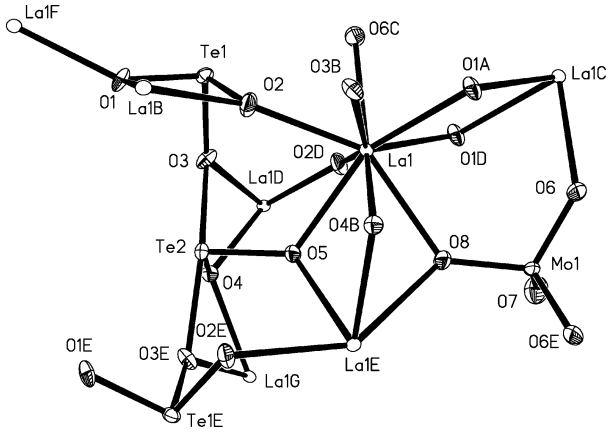

Figure 5. ORTEP representation of the selected unit in $La_2MoTe_3O_{12}$. The thermal ellipsoids are drawn at 50% probability. Symmetry codes for the generated atoms: (a) $-x + 1/2, -y + 1, z + 1/2$; (b) $x + 1/2, y, -z + 1/2$ (c) $-x, -y + 1, -z + 1$; (d) $x - 1/2, y, -z + 1/2$; (e) $x, -y + 3/2, z$; (f) $-x + 1/2, -y + 1, z - 1/2$; (g) $x - 1/2, -y + 3/2, -z + 1/2$.

in A_2SeMoO_6 (A = Na, K, Rb).[15] Such distortion is due to the second-order Jahn−Teller effects of the octahedrally coordinated d^0 metals, which are reinforced by the lone pair Se^{4+} cations.[14] Bond valence calculations indicate that the Mo atom is in an oxidation state of +6 and the Se atoms are +4; the calculated total bond valences for Mo(1), Se(1), Se(2), and Se(3) are 5.99, 3.88, 3.89, and 3.88, respectively.[11]

The $Se(1)O_3$ group is a pentadentate metal linker: it chelates bidentately with a Gd(2) atoms and also bridges with one Gd(1), one Gd(2), and one Mo(1) atom. The $Se(2)O_3$ group bridges with 4 Gd(1), 1 Gd(2), and 1 Mo(1). The $Se(3)O_3$ group acts as a pentadenate group and is bonded to 2 Gd(1), 2 Gd(2) and 1 Mo(1). The interconnection of the Gd^{III} ions by selenite groups results in a 3D network with tunnels running along the *b* axis (Figure 4). The MoO_6 octahedra are located at the tunnels formed by the gadolinium(III) selenite (Figure 4).

$La_2MoTe_3O_{12}$ and $Nd_2MoTeO_3O_{12}$ were obtained in our attempts to prepare the tellurium(IV) analogue of $Gd_2MoSe_3O_{12}$. Although their chemical compositions are comparable to that of $Gd_2MoSe_3O_{12}$, each of them belongs to a unique structural type. $La_2MoTe_3O_{12}$ has a three-dimensional network structure whereas $Nd_2MoTe_3O_{12}$ is layered.

The structure of $La_2MoTe_3O_{12}$ is composed of two La^{3+} ions, one MoO_4^{2-} anion, and one $Te_3O_8^{4-}$ anion (Figure 5). It can be viewed as two selenite groups in $Nd_2MoSe_2O_{10}$

(12) Galy, J.; Meunier, G.; Andersson, S.; Åström, A. *J. Solid State Chem.* **1975**, *13*, 142.
(13) Wickleder, M. S.; Goehausen, I. *Z. Anorg. Allg. Chem.* **2000**, *626*, 1725.
(14) Halasyamani, P. S. *Chem. Mater.* **2004**, *16*, 3586.
(15) Wong, W.-K.; Liang, H.-Z.; Guo, J.-P.; Wong, W.-Y.; Lo, W.-K.; Li, K.-F.; Cheah, K.-W.; Zhou, Z.-Y.; Wong, W.-T. *Eur. J. Inorg. Chem.* **2004**, 829.

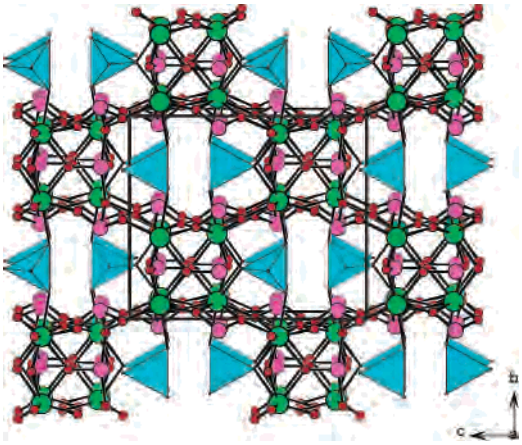

Figure 6. View of the structure of $La_2MoTe_3O_{12}$ down the *a* axis. The MoO_4 tetrahedra are shaded in cyan. La, Te, and O atoms are drawn as green, pink, and red circles, respectively.

being replaced by a $Te_3O_8^{4-}$ anion. The La^{3+} ion is 9-coordinated by 7 oxygen atoms from 4 $Te_3O_8^{4-}$ anions (one of them in a unidentate fashion, two of them forming two La−O−Te−O four membered chelating rings, and the other one forming a La−O−Te−O−Te−O six-member chelating ring) and two oxygen atoms from two MoO_4^{2-} anions. The La−O distances range from 2.451(8) to 2.821(8) Å (Table 2). Te(1) is 3-coordinated whereas Te(2) is 4-coordinated. The $Te(2)O_4$ group connects with two $Te(1)O_3$ groups through corner-sharing (O(3)) to form a $Te_3O_8^{4-}$ polytellurium(IV) oxide anion. The Te−O distance of the Te−O−Te bridge (2.183(7) Å) is significantly longer than the remaining Te−O bonds (1.848(8)−1.898(8) Å). Similar to that in $Nd_2MoSe_2O_{10}$, the Mo atom is in a tetrahedral coordination geometry. The Mo−O distances range from 1.754(8) to 1.793(11) Å, which are comparable to those in $Nd_2MoSe_2O_{10}$. The oxidation states of Mo and Te atoms are +6 and +4, respectively, which are supported by the results of bond valence calculations.[11] The calculated total bond valences for Mo(1), Te(1), and Te(2) are 5.89, 4.03, and 3.78, respectively. The interconnection of the lanthanum(III) by chelating and bridging $Te_3O_8^{4-}$ anions leads to a three-dimensional network with tunnels along the *a* axis. These tunnels are formed by 20-membered rings (6 La, 4 Te, and 10 O atoms). The MoO_4 polyhedra are located at the above tunnels and connected with the La^{3+} ions via corner sharing (Figure 6).

$Nd_2MoTe_3O_{12}$ can also be formulated to be $Nd_2(MoO_4)(TeO_3)(Te_2O_5)$; it can be considered as the $Te_3O_8^{4-}$ anion in $La_2MoTe_3O_{12}$ being replaced by a tellurite group and a ditellurite group. Different from the La(III) ion in $La_2MoTe_3O_{12}$, the Nd(III) ion in $Nd_2MoTe_3O_{12}$ is 8-coordinated by eight oxygen atoms (Figure 7). The Nd−O distances in the range of 2.324(4)−2.603(4) Å are comparable to those in $Nd_2MoSe_2O_{10}$. The Te atoms in the tellurite and ditellurite groups are each coordinated by three oxygen atoms, and their coordination geometries can also be described as a TeO_3 trigonal pyramid in which the Te atom resides in the pyramidal site. The Te−O distances are in the range 1.838(4)−1.987(2) Å (Table 2). The O6 atom bridging with two Te atoms in the ditellurite group has the longest Te−O

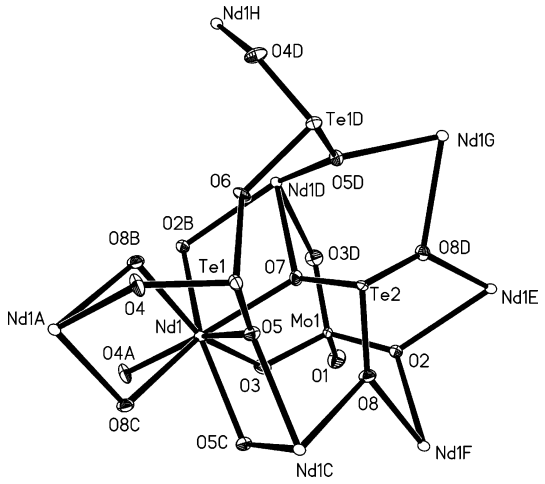

Figure 7. ORTEP representation of the selected unit in $Nd_2MoTe_3O_{12}$. The thermal ellipsoids are drawn at 50% probability. Symmetry codes for the generated atoms: (a) $-x+1, -y, -z+2$; (b) $x, y, z+1$; (c) $-x+1, -y, -z+1$; (d) $x, -y+1/2, z$; (e) $x, -y+1/2, z-1$; (f) $x, y, z-1$.

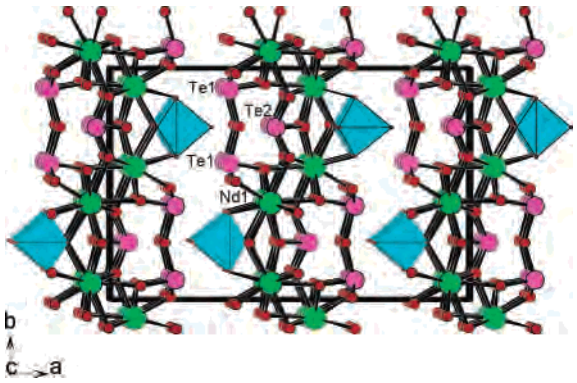

Figure 8. View of the structure of $Nd_2MoTe_3O_{12}$ down the *c* axis. The MoO_4 tetrahedra are shaded in cyan. Nd, Te, and O atoms are drawn as green, pink, and red circles, respectively.

distance (1.987(2) Å). Unlike the metal diselenites, reports on metal ditellurites are much fewer.[1,5,6] In addition to the $Te_3O_8^{4-}$ anion in $La_2MoTe_3O_{12}$ and ditellurite anion in $Nd_2MoTe_3O_{12}$, the Te(IV) ion can also form several other polymeric units such as the $Te_2O_6^{4-}$ anion in $CeTe_2O_6$ and the linear $Te_4O_{11}^{6-}$ anion in $Ln_2Te_4O_{11}$ (Ln = La−Lu).[1,6] Similar to those in $Nd_2MoSe_2O_{10}$ and $La_2MoTe_3O_{12}$, the Mo atom is in a tetrahedral coordination geometry with Mo−O distances ranging from 1.716(6) to 1.802(5) Å. The oxidation states of Mo and Te are +6 and +4, respectively, which are supported by the results of bond valence calculations.[11] The calculated total bond valences for Mo(1), Te(1), and Te(2) are 5.81, 3.69, and 3.81, respectively.

The interconnection of Nd(III) ions by bridging tellurite and ditellurite groups lead to ⟨100⟩ and ⟨200⟩ layers (Figure 8). Each tellurite anion bridges with six Nd(III) ions, whereas the ditellurite anion bridges with five Nd(III) ions. The MoO_4 tetrahedron is connected to four Nd(III) ions within the 2D layer, and the terminal O(1) atom is orientated to the interlayer space (Figure 8). The interlayer distance is about 8.85 Å.

IR spectra of the four compounds show Mo^{6+}−O stretching bands at 918−933 cm and 840−852 cm^{-1}. IR spectra of $Nd_2MoSe_2O_{10}$ and $Gd_2MoSe_3O_{12}$ exhibit the characteristic

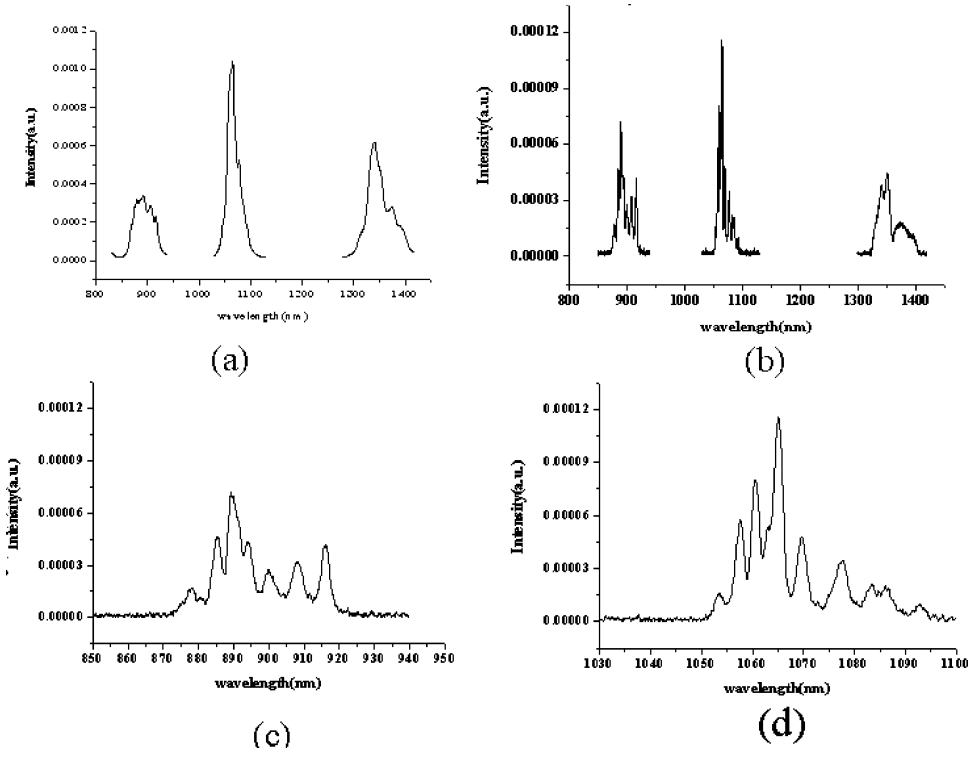

Figure 9. Solid state emission spectrum of $Nd_2MoSe_2O_{10}$ under excitation at $\lambda_{ex} = 514$ nm at (a) room temperature and(b) 10 K. The enlarged views of the emission bands for (c) $^4F_{3/2} \rightarrow {}^4I_{9/2}$ and (d) $^4F_{3/2} \rightarrow {}^4I_{11/2}$ at 10 K.

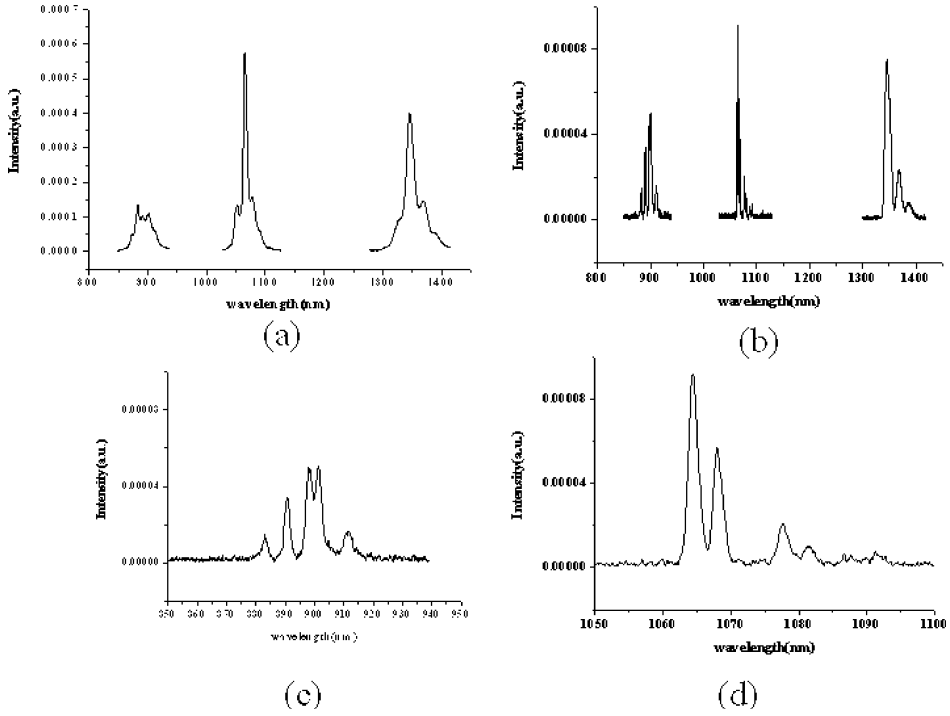

Figure 10. Solid state emission spectrum of $Nd_2MoTe_3O_{12}$ under excitation at $\lambda_{ex} = 514$ nm at (a) room temperature and (b) 10 K. The enlarged views of the emission bands for (c) $^4F_{3/2} \rightarrow {}^4I_{9/2}$ and (d) $^4F_{3/2} \rightarrow {}^4I_{11/2}$ at 10 K.

vibrations ν(Se−O) in the region from 896 to 740 cm^{-1}. IR spectra of $La_2MoOTe_3O_{12}$ and $Nd_2MoTe_3O_{12}$ reveal Te−O stretch bands at 783 and 639 cm^{-1}, and the vibrations at 580 and 466 cm^{-1} can be assigned to M−O−Te bonds.[2a]

Luminescent Properties. The solid state luminescent properties of $Nd_2MoSe_2O_{10}$, and $Nd_2MoTe_3O_{12}$ were investigated both at room temperature and 10 K. Their emission spectra are shown in Figures 9 and 10, respectively. Under excitation at 514 nm, both compounds display three sets of characteristic emission bands for the Nd(III) ion in the near-IR region (Table 3): $F_{3/2} \rightarrow {}^4I_{9/2}$, $^4F_{3/2} \rightarrow {}^4I_{11/2}$, and $^4F_{3/2} \rightarrow {}^4I_{13/2}$.[15,16] It should be noted that the intensity of the $^4F_{3/2} \rightarrow {}^4I_{13/2}$ band in all spectra cannot be compared with those of the other two bands due to two different grating used (1200

Table 3. Observed Emission Bands (nm) for $Nd_2MoSe_2O_{10}$ and $Nd_2MoTe_3O_{12}$ at Room Temperature and 10 K

	$Nd_2MoSe_2O_{10}$		$Nd_2MoTe_3O_{12}$	
	RT	10 K	RT	10 K
$^4F_{3/2} \rightarrow {}^4I_{9/2}$	880.5, 894.0, 907.0, 917.5	878.7, 880.9, 885.6, 889.5, 894.5, 900.1, 908.5, 916.4	885.5, 893.5, 904.5	883.4, 890.9, 898.3, 901.8, 912.1
$^4F_{3/2} \rightarrow {}^4I_{11/2}$	1066.0, 1078.5	1053.9, 1057.9, 1060.9, 1063.7, 1065.4, 1070.1, 1078.1, 1083.7, 1086.3, 1093.9	1055.5, 1067.0, 1081.0	1064.6, 1068.1, 1077.9, 1082.0, 1086.8, 1091.5
$^4F_{3/2} \rightarrow {}^4I_{13/2}$	1342.0, 1376.5	1342.2, 1351.8, 1373.4	1349.0, 1373.0	1347.2, 1369.3, 1388.9

line/mm grating for the 850−1125 nm range and 300 line/mm grating for the 1300−1450 nm range). Studies performed by using these two different gratings in the 1025−1250 nm region indicate that luminescence intensity obtained by using the 1200 line/mm grating is approximately 75% of that obtainedwith the 300 line/mm grating (see Supporting Information). $Nd_2MoTe_3O_{12}$ contains only one independent Nd(III) site whereas $Nd_2MoSe_2O_{10}$ contains two unique Nd(III) sites, all of them are in the C_1 symmetry. Due to the crystal field effect, each transition band was split into several subbands (Table 3). The $^4F_{3/2}$ band is expected to split into two sublevels whereas the complete degeneracy of $^4I_{9/2}$, $^4I_{11/2}$, and $^4I_{13/2}$ leads to 5, 6, and 7 sublevels, respectively.[17] Therefore, $^4F_{3/2} \rightarrow {}^4I_{9/2}$, $^4F_{3/2} \rightarrow {}^4I_{11/2}$, and $^4F_{3/2} \rightarrow {}^4I_{13/2}$ transitions will have a maximum of 10, 12, and 14 subbands if both the lower and upper levels of $^4F_{3/2}$ are populated. When two and more unique Nd(III) sites are present such as $Nd_2MoSe_2O_{10}$, the spectrum will be even more complicated. Due to the overlapping of some emission bands and resolution limit of the instruments, the observed emission peaks are usually fewer than that expected (Table 3). At very low temperatures such as 10 K, the lower level of $^4F_{3/2}$ is the most likely populated one; hence, the corresponding emission spectra have much better resolution (Figures 9 and 10). The low temperature emission spectrum for $Nd_2MoTe_3O_{12}$ displays 5 and 6 subbands for the $^4F_{3/2} \rightarrow {}^4I_{9/2}$ and $^4F_{3/2} \rightarrow {}^4I_{11/2}$ transitions, respectively, which is in good agreement with theoretical expectations. Assuming the energy the lowest sublevel of $^4I_{9/2}$ is 0 cm^{-1}, the energy of the lower level of $^4F_{3/2}$ is calculated to be 11320 cm^{-1}, and the energies of the other four sublevels for $^4I_{9/2}$ are 95.0, 188, 231, and 356 cm^{-1}, respectively. Likewise, we can calculate the energies for the six sublevels of $^4I_{11/2}$, which are 1927, 1958, 2043, 2078, 2119, and 2158 cm^{-1}, respectively. The energy calculations for $^4I_{13/2}$ sublevels are difficult due to the incompleteness of the degeneracy of its sublevels, and so are the calculations of the sublevels in $Nd_2MoSe_2O_{10}$ with two unique Nd(III) ions in C_1 symmetry. The lifetimes for the $^4F_{3/2} \rightarrow {}^4I_{9/2}$ transition (YAG laser 335 nm excitation, monitor wavelength 875 nm with PMT detector) were determined to be 0.21 and 0.20 ms for $Nd_2MoSe_2O_{10}$ and $Nd_2MoTe_3O_{12}$, respectively. The lifetimes for the $^4F_{3/2} \rightarrow {}^4I_{9/2}$ transition were not measured due to the limitation of the instrument used.

Magnetic Properties. Magnetic properties for $Nd_2MoSe_2O_{10}$ and $Nd_2MoTe_3O_{12}$ have been studied at a magnetic field of 10000 Oe in the temperature range 2−300 K. Both compounds are paramagnetic over the whole experimental temperature range. Since Mo(V), TeO_3^{2-}, $Te_2O_5^{2-}$, and SeO_3^{2-} are diamagnetic, the paramagnetic contribution is expected to come solely from the Nd^{3+} ions. At 300 K, the measured $\chi_m T$ values are 2.97 and 2.74 emu·K·mol^{-1}, respectively, for $Nd_2MoSe_2O_{10}$ and $Nd_2MoTe_3O_{12}$. Hence, the effective magnetic moments (μ_{eff}'s) are calculated to be 4.88 and 4.68 μ_B, respectively, for $Nd_2MoSe_2O_{10}$ and $Nd_2MoTe_3O_{12}$, which are slightly smaller than the theoretical values (both are 5.2 μ_B). At 2 K, the $\chi_m T$ values are decreased to 1.03 and 0.89 emu·K·mol^{-1}, respectively, for $Nd_2MoSe_2O_{10}$ and $Nd_2MoTe_3O_{12}$, indicating the antiferromagnetic interactions between Nd(III) centers.

Plots of χ_m^{-1} versus T indicate that both compounds obey the Curie−Weiss law above 30 K, but slight deviation is observed below this temperature (see Supporting Information). Linear fitting of χ_m^{-1} with T above 100 K gave Weiss constants of −32(2) and −23(1) K, respectively, for $Nd_2MoSe_2O_{10}$ and $Nd_2MoTe_3O_{12}$, indicating significant antiferromagetic interactions between Nd(III) ions in both compounds. The shortest Nd−Nd distance of 3.820(1) Å in $Nd_2MoSe_2O_{10}$ is slightly shorter than that of 3.870(1) Å in $Nd_2MoTe_3O_{12}$, which is probably responsible for the stronger magnetic interactions in $Nd_2MoSe_2O_{10}$. Another fact may be related to the stronger magnetic interaction in $Nd_2MoSe_2O_{10}$ is that the structure of $Nd_2MoSe_2O_{10}$ is a close-packing 3D network whereas that of $Nd_2MoTe_3O_{12}$ is a more opened 2D layer. More detailed calculations of these magnetic interactions were not performed due to the complexity of the structures as well as the lack of suitable models.

Conclusion

In summary, the syntheses, crystal structures, IR, and luminescent properties of four new rare-earth selenites or telluites containing additional MoO_4 tetrahedra or MoO_6 octahedra have been described. Their structures can be viewed as lanthanide selenite or tellurium(IV) oxide-based open frameworks being decorated by MoO_4 tetrahedra or MoO_6 octahedra. The MoO_4 tetrahedra in $Nd_2MoSe_2O_{10}$ form a 2D layer with Nd(III) ions, and the MoO_4 tetrahedra in $Nd_2MoTe_3O_{12}$ act as pendant groups between the 2D layers of lanthanide tellurium(IV) oxide. The MoO_6 octahedra in $Gd_2MoSe_3O_{12}$ are located at the tunnels formed by lanthanide(III) selenite, whereas the MoO_4 tetrahedra in La_2-

(16) (a) Song, J.-L.; Lei, C.; Mao, J.-G. *Inorg. Chem.* **2004**, *43*, 5630. (b) Hebbink, G. A.; Grave, L.; Woldering, L. A.; Reinhoudt, D. N.; van Vegel, F. C. J. M. *J. Phys. Chem.* **2003**, *A107*, 2483. (c) Faulkner, S.; Pope, S. J. A. *J. Am. Chem. Soc.* **2003**, *125*, 10526. (d) Pope, S. J. A.; Kenwright, A. M.; Boote, V. A.; Faulkner, S. *J. Chem. Soc., Dalton Trans.* **2003**, 3780.

(17) Morrison, C. A.; Leavitt, R. P. Spectroscopic properties of triply ionized lanthanides in transparent host crystals. In *Handbook on the Physics and Chemistry of Rare Earth*; Gschneider, K. A., Eyring, L., Eds.; North-Holland Publishing Company:New York, 1982; Vol. 5, pp 461−693 and references therein.

$MoTe_3O_{12}$ are located at the tunnels of $\{La_2(Te_3O_8)\}^{2+}$ ions. Luminescent studies indicate that $Nd_2MoSe_2O_{10}$ and $Nd_2MoTe_3O_{12}$ are possible candidates for 1.06 μm emission. We believe that other new lanthanide luminescent compounds can be developed by applying two types of inorganic anions as luminescent activators for lanthanide(III) ions.

Acknowledgment. This work was supported by the National Natural Science Foundation of China (20371047) and NSF of Fujian Province (E0420003).

Supporting Information Available: X-ray crystallographic files and XRD powder patterns for $Nd_2MoSe_2O_{10}$, $Gd_2MoSe_3O_{12}$, $La_2MoTe_3O_{12}$, and $Nd_2MoTe_3O_{12}$, plots of $\chi_m T$ versus T and χ_m^{-1} versus T for $Nd_2MoSe_2O_{10}$ and $Nd_2MoTe_3O_{12}$, as well as the luminescent lifetime measurements and the comparison of the luminescence intensity for the $^4F_{3/2} \rightarrow {}^4I_{11/2}$ transition at two different gratings. This material is available free of charge via the Internet at http://pubs.acs.org.

IC051376M